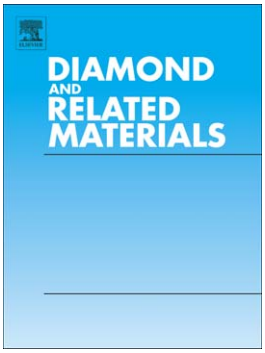


# New electrochemically improved tetrahedral amorphous carbon films for biological applications

Tomi Laurila, Vera Protopopova, Sneha Rhode, Sami Sainio, Tommi Palomäki, Michelle Moram, Juan M. Feliu, Jari Koskinen

PII: S0925-9635(14)00165-4
DOI: doi: 10.1016/j.diamond.2014.08.007
Reference: DIAMAT 6295

To appear in: *Diamond & Related Materials*

Received date: 8 May 2014
Revised date: 13 August 2014
Accepted date: 18 August 2014

Please cite this article as: Tomi Laurila, Vera Protopopova, Sneha Rhode, Sami Sainio, Tommi Palomäki, Michelle Moram, Juan M. Feliu, Jari Koskinen, New electrochemically improved tetrahedral amorphous carbon films for biological applications, *Diamond & Related Materials* (2014), doi: 10.1016/j.diamond.2014.08.007

# New electrochemically improved tetrahedral amorphous carbon films for biological applications

Tomi Laurila[1*], Vera Protopopova[2], Sneha Rhode[3], Sami Sainio[1], Tommi Palomäki[1], Michelle Moram[3], Juan M. Feliu[4] and Jari Koskinen[2]

[1] Department of Electrical Engineering and Automation, School of Electrical Engineering, Aalto University, Espoo, Finland

[2] Department of Materials Science and Engineering, School of Chemical Technology, Aalto University, Espoo, Finland

[3] Department of Materials, Faculty of Engineering, Imperial College, London, UK

[4] Institute of Electrochemistry, University of Alicante, Spain

**Abstract**

Carbon based materials have been frequently used to detect different biomolecules. For example high $sp^3$ containing hydrogen free diamond-like carbon (DLC) possesses many properties that are beneficial for biosensor applications. Unfortunately, the sensitivities of the DLC electrodes are typically low. Here we demonstrate that by introducing topography on the DLC surface and by varying its layer thickness, it is possible to significantly increase the sensitivity of DLC thin film electrodes towards dopamine. The electrode structures are characterized in detail by atomic force microscopy (AFM) and conductive atomic force microscopy (C-AFM) as well as by transmission electron microscopy (TEM) combined with electron energy loss spectroscopy (EELS). With cyclic voltammetry (CV) measurements we demonstrate that the new improved DLC electrode has a very wide water window, but at the same time it also exhibits fast electron transfer rate at the electrode/solution interface. In addition, it is shown that the sensitivity towards dopamine is increased up to two orders of magnitude in comparison to the previously fabricated DLC films, which are used as benchmarks in this investigation. Finally, it is shown, based on the cyclic voltammetry measurements that dopamine exhibits highly complex behavior on top of these carbon electrodes.

*Corresponding author. Tel: +358503414375 email: tomi.laurila@aalto.fi

## 1. Introduction

Monitoring the state of the human body and its functions by network of wirelessly interconnected sensors is a scientific, economic and technological challenge of utmost importance. If combined with the ability to stimulate these sensor/actuator networks could act as the user interface between living and electronic worlds. At this specific interface the information can be gathered by a network of sensors. In the case of electrochemical sensors, the electrode is the element which is in immediate contact with the biological environment. Thus, the operation of the interface between biological system and electronic device relies on the functionality of this electrode.

The rate of the electrochemical reactions is significantly influenced by the nature of the electrode surface [1]. The kinetics of oxygen and hydrogen evolution is significantly slower on carbon than on most commonly used metal electrodes [2]. The resulting wide potential window is one of the reasons for the widespread use of carbon materials for electrodes. Amorphous diamond-like carbon (DLC), is a non-crystalline carbon with high fraction of diamond-like ($sp^3$) bonds [3]. DLC coatings are characterized by excellent physical properties (high hardness, high elastic modulus) as well as chemical inertness to any acids, alkaline solutions, and organic solvents [3]. We have recently shown that DLC electrodes are exceptionally stable in phosphate buffered saline (PBS) solution, but can still be utilized to detect biomolecules by inducing local electrochemically active spots on the otherwise inert DLC electrode [4]. Furthermore, DLC in its many forms is an attractive electrode material because of its antifouling properties and general biocompatibility [5-17].

Neurotransmitters, such as dopamine, provide the important communication link between neurons. Abnormal dopamine transmission has been associated with several neurological disorders, e.g. Parkinson's disease, schizophrenia, and Huntington's disease [18]. For therapeutic purposes, an accurate determination of dopamine level in situ would be highly desirable. When dopamine is oxidized two electrons and two protons are transferred [2,19,20]. These electrons can be detected with cyclic voltammetry, for instance. The primary challenge here is that the concentration of dopamine in the extracellular fluid is very low (0.01 -1 μM) [20]. Secondly, the released dopamine is rapidly cleared from the extracellular space. Thus, the sensor must not only be sensitive and selective, but it should also have a fast response time. The third challenge is long term stability, which is confronted by the adsorption of oxidation products leading to the fouling of the electrode.

As stated above, the motivation to use DLC thin films as bioelectrodes lies for example in their biocompatibility, easy processability, compatibility with current CMOS processes, mechanical

robustness, and excellent corrosion resistance. Unfortunately, the sensitivity of DLC coated electrodes towards, for example dopamine, is typically not high enough if other more electrochemically active materials are not combined with the DLC matrix [4]. The purpose of this work is to show that by utilizing a specific deposition process for DLC thin film electrode system, it is possible to achieve not only chemically very inert, but *at the same time* electrochemically active electrode material. The microstructure as well as the electrochemical properties of the DLC films will be characterized in detail. Here our previous DLC coatings with approximately the same $sp^3$ content will be used as the benchmark. The main differences between the two coatings will be discussed and the factors most likely contributing to the observed very different electrochemical behavior will be rationalized.

## 2. Experimental

The substrate materials used were either p- or n-type Si(100) wafers (Ultrasil and Okmetic). Two different kinds of samples were fabricated for the electrochemical investigations. In both cases the samples consisted of Ti interlayer and layer of tetrahedral amorphous carbon, although different types of processing conditions and experimental setup were used.

In the first case, direct current (DC) magnetron sputtering system and dual filtered cathodic arc deposition system were used for titanium and carbon deposition, respectively. It is to be noted that both systems are installed in one deposition chamber. The highly conductive p-type boron-doped (100) Si wafers with 0.001–0.002 Ohm·cm resistivity were utilized. All wafers were cleaned by standard RCA-cleaning procedure before the deposition. Samples were placed in the rotating holder (rotational velocity used was 20 rpm). The vacuum in the chamber was pumped down by dry scroll vacuum pump (Edwards XDS10) and by cryo pump Cryo-Torr (Helix Technology corporation). In order to achieve a low vacuum, a high vacuum throttle valve was used. DC-magnetron sputtering system was equipped by circular and water-cooled magnetron sputtering source with 2 inch Ti target (Kurt J. Lesker Company) and DC generator (DCO2 BP). The shutter was utilized for controlling the sputtering time. Pre-sputtering of 2 min was carried out for cleaning the surface of Ti target. Titanium interlayers were deposited under the following deposition conditions: discharge power was fixed at 100 W, total pressure was 0.67 Pa, Ar gas flow rate was 28 sccm, deposition temperature was close to room temperature, and deposition time was 350 s. Cathodic arc deposition system purchased from Lawrence Berkeley National Laboratory was equipped the $90^o$ bent magnetic filter for the reduction of the macroparticle contamination. Two 99.997 % graphite rods (Goodfellow) of the diameter of 6.35 mm were used as the carbon cathodes,

which were surrounded by a cylindrical anode. The arc current pulses had the amplitude of 0.7 kA and 0.6 ms pulse width. Each pulse was triggered at 1 Hz frequency. The 2.6 mF capacitor bank was charged to 400 V. Number of pulses was 360. The distance between the substrate holder and the filter was about 20 cm. Total pressure during the deposition process was no less than $1.3 \cdot 10^{-4}$ Pa. These electrodes are marked in the subsequent analyses as improved ta-C (IMP-ta-C).

In the second case, the deposition was done by using another experimental set-up. The 70 l deposition chamber was pumped with an oil diffusion pump to base pressure of $1x10^{-3}$ Pa. The samples were mounted by hanging in rotating carrousel with planetary rotation of the substrate holders. The full rotation time of the carrousel was about 25 s. The chamber has two arc sources and one ion source on the chamber walls. Prior to deposition the samples were etched by using a griddles argon ion source. The titanium coating was deposited by using a continuous current arc source equipped with 60° magnetic filtering. The arc current used was 55A and the duration of the deposition was 35 s. For the carbon a 2.6 mF capacitor bank was charged to 200 V and the arc was triggered with ignition electrodes. The maximum pulse current was 3 kA and the pulse width was about 0.3 ms. Each pulse was triggered separately at 1 Hz frequency. The deposition rate during the pulse was about $1.4x10^{15}$ ions/cm$^2$, as measured from the growth rate of a carbon layer on a flat silicon substrate. The distance from the cathode varied between 150 to 300 mm during the deposition due to sample rotation. The average carbon ion energy has been previously measured to be 40 – 50 eV using an electrostatic probe. It may be assumed that all carbon in the plasma is ionized. These electrodes are subsequently marked as reference ta-C (REF-ta-C).

The morphology of the fabricated samples was studied with optical microscopy (Leica), and scanning electron microscopy SEM (Hitachi-4700). Scanning probe microscope Ntegra Aura (NT-MDT Company) with variable measuring facilities was used to carry out atomic force microscopy (AFM), spreading resistance microscopy or in other words conductive-AFM (SRM or C-AFM) and current-voltage spectroscopy, as well as scanning tunneling microscopy (STM). The measurements were carried out in ‘scanning by sample’ mode with the use of two different measuring heads. In the case of conductive AFM, a diamond coated conductive probe (DCP10) was mounted to special probe holder designed for the current measurements under the varied voltage applied to the probe. The measurements were performed in the contact regime. The typical curvature of radius of the tip used was about 100 nm and the force constant of the cantilvers was nominally 11.5 N/m. In the case of STM measurements, STM head and TT10 Bruker etched tungsten tip (length was 8 mm, diameter was 0.25 mm) were used. Tip height was chosen to give the tip current 0.2 nA under the tip (bias) voltage of 0.5 V. Dependencies of the tunneling current on the voltage applied to the

sample were obtained from STM. In both cases of current-voltage characteristics measurements, dependences were the average of, at least, 50 measurements in different points. Bitmap images (topography and current maps) were processed with free software Gwiddion 2.34.

Samples were further characterized by X-ray reflection (XRR) analysis performed *via* Philips X'Pert Pro diffractometer (CuKα, λ = 1.5405 Å, acceleration voltage 40 kV, anode current 40 mA) and visible Raman spectroscopy with the use of WITec alpha 300 spectrometer (laser wave length was 532 nm, exposure time was 0.1 s, and spectrum wave number was in the range of 450 to 3900 cm-1). All spectra obtained were processed by an averaging of 100 spectra and a background subtraction. The thickness of deposited layers was measured by means of profilometer (Dektac).

Cross-sectional TEM samples were prepared conventionally by grinding, polishing and dimpling the specimen until its thickness was below 10 microns, followed by Ar ion milling performed using a PIPS Ion miller (Gatan USA). High-resolution transmission electron microscopy (HRTEM) was performed using a double-aberration-corrected JEOL 2200FS microscope and a JEOL 2100 (JEOL, Japan) microscope equipped with a field emission gun (FEG) operating at 200 kV. Moreover, the JEOL 2100 microscope was used to perform scanning transmission electron microscopy (STEM) using high angle annular dark-field (HAADF) imaging. The JEOL 2200FS TEM was equipped with an energy dispersive x-ray (EDX) spectrometer for elemental analysis and the JEOL 2100 was equipped with the Gatan image filter (GIF) for electron energy-loss spectroscopy (EELS). A Gatan 4k×4k UltraScan 4000 CCD camera was employed for digital recording of the HRTEM images.

Cyclic voltammetry (CV) was carried out with Gamry Reference 600 Potentiostat/Galvanostat/ZRA. Contact was made to the backside of the sample by using Cu wire and Ag adhecive. The sample was placed inside a polycarbonate sample holder which protected completely the sides and back of the electrode. Hole with a diameter of 8 mm in the sample holder allowed the solution to reach contact with the electrode. Water window was measured in 0.15 M sulfuric acid and the dopamine measurements utilized different concentrations of dopamine in phosphate buffered saline (PBS) solution. Sweep rate was typically set to 50 mV/s. The reference electrode was Ag/AgCl skinny reference electrode provided by Sarissa Biomedical ltd, pH values of the $H_2SO_4$ and PBS solutions were, 0.55 and 7.4, respectively. All the solutions were deoxygenated with $N_2$ for 5 min prior to measurement and the air in the electrochemical cell was purged with $N_2$ during the measurements. All the measurements were conducted at room temperature. The dopamine solutions were always prepared on the day of the measurement, because it is easily

oxidized in air. A 10 mM dopamine solution was prepared by dissolving 0.18964 g of dopamine hydrochloride (Sigma-Aldrich, St. Louis, USA) in 100 mL of phosphate-buffered saline (PBS Dulbecco, Biochrom AG, Berlin, Germany) that was diluted to obtain a series of dopamine solutions from a concentration of 1 mM to 1 nM. Ferrocenemethanol (FcMeOH) was used as an outer-sphere redox system to define the electron transfer rate of the given electrode. The measurements were conducted in 1 mM FcMeOH solution obtained by dissolving 0.02227 g of 97% ferrocenemethanol (Sigma-Aldrich, St. Louis, USA) in 100 mL of 0.15 M sulfuric acid (Merck kGaA, Darmstadt, Germany). These solutions were also freshly prepared, because FcMeOH is easily oxidized in air. The measurements were carried out at scan rates of 10, 50, 100, 200 and 400 mV/s.

## 3. Results and Discussion

### *3.1 Microstructural properties*

The results from the optical microscopy combined with the SEM investigations show that the surface of IMP-ta-C and REF-ta-C are both very uniform, smooth and lack any kind of large scale structural features on the average. However, the results of local roughness measurements by means of AFM (Figure 1) indicate that the first sample (IMP-ta-C) has a rougher surface, characterized by the average roughness of about 1.6 nm, than the second sample (REF-ta-C), with the average roughness equal to about 0.32 nm. It is to be noted here that the Ti adhesion layer, even though equal in thickness (20 nm) was deposited with DC magnetron sputtering in the case of IMP-ta-C and cathodic arc in the case of REF-ta-C. It is likely that the two different deposition methods for Ti interlayer will result into different morphology of the adhesion layer underneath the two types of DLC's. As the DLC is known to form highly conformal coatings, the appearance of the roughness difference between the two types of films can be expected to be caused by the different roughness of Ti interlayers. This fact is supported by SEM and cross-sectional TEM images, which illustrated that the morphology of DLC films more or less replicated the morphology of Ti layer (see below). Also the AFM measurements carried out only for the Ti layer on top of Si substrates (not shown here) were consistent with the above reasoning.

It seems, however, unlikely that drastically different electrochemical behavior seen later on could be totally explained only by the different surface roughness and resulting increase in the surface area. One factor that may play an important role in the different electrochemical performance is the surface electrical properties of the two types of samples, including local electrical properties. It is to be noted that the use of different deposition methods, magnetron

sputtering and cathodic arc deposition for the Ti layers, will lead, not only to variation in surface roughness, but also to dissimilar crystalline structure and purity of the Ti adhesion layer, which may have effects on the sensing properties of the DLC electrodes. It should be noted, however, that there are also other possible reason(s) of different electrochemical behavior of electrodes, including the possible differences in electronic structure of the two DLC layers caused by usage of different deposition equipment. In order to find out if there are in fact differences, for example, in the local electrical properties between the two electrode structures, conductive AFM measurements were carried out.

Topography and simultaneous current maps from both samples are shown in Figure 1 (a, b, d, e). One can notice by comparing Figures 1 (a) and (b) that the highest surface locations correlate with the low current values, especially in the case of the first (IMP-ta-C) sample. This is further confirmed by matching of the profiles from the topography and measured currents shown in Figure 1 (c) and (f). It should be noted that the brightest features in Figure 1 (a) are not caused by contamination or dust, because they stayed on the surface even after acetone ultrasonication. They are expected to be caused either by features of the underneath Ti layer (which is highly probable, because their size is the same as other surface features), or by particles, which are not fully filtered out by magnetic filter during cathodic arc deposition. Observed current variation (in the case of IMP-ta-C sample) can be correlated with the different mechanical contact established between the probe and the real rough surface [21]. Mechanical properties of the contact can be described with the use of Hertz elastic contact theory [21-23] and ball-ball approximation. Our estimations [24] made for the real geometry (the probe radius of 100 nm, the width and the height of the each surface grain 150 nm and 1 nm, respectively) show that, if the probe is in the contact with the top or the lateral surface of the grain, the contact radius is 10 nm and the contact area is 314 $nm^2$. However, if the probe is located in the valley and in the contact with two adjacent grains, the contact radius and the contact area are twice as large. This estimation clearly demonstrates the reason why we can observe more current in the valleys in comparison to the hills of the surface. It is also consistent with the fact that current variations are not observed in the case of the sample with the smoother surface (REF-ta-C). But the average current flowing through the REF-ta-C sample is almost one order of magnitude less in comparison with IMP-ta-C, which indicate different current conduction mechanisms through the two ta-C layers.

The model of space-charge-limited (SCL) currents [25,26] is widely used for the explanation of conduction mechanism through dielectrics, depending on which current-voltage curves can be approximated by a power function $I \approx U^N$ with different power values $N$. In the simplest case (under

the weak electrical field), current-voltage curves are expressed as Ohm's law (with exponent N=1). Increasing the voltage value leads to shift from Ohm's law to the power law dependence connected with the existence of traps in the band gap. In the case of the monoenergetic traps, a quadratic law can be observed. In the case, when traps have an exponential energy distribution, current-voltage dependences are more complicated and are described by power law dependence with exponent values more than 3. As it is noticed from current-voltage spectroscopy data (Figure 2) acquired by means of conductive AFM, the power values for IMP-ta-C and REF-ta-C are equaled to 2.14 and 2.8-4.3, respectively. Estimated trap energy for IMP-ta-C and REF-ta-C are 0.029 and 0.047-0.085 eV. Thus, in both cases, the current conduction mechanism can be described in terms of space-charge-limited current. However, it is caused by two different trap mechanisms, which are either monoenergetic traps present in IMP-ta-C or by exponentially distributed ones in REF-ta-C. In addition, the slope values between 4 to 6 are typical to the oxide layers [27,28] which indirectly proof that Ti layer deposited via cathodic arc deposition contains more oxygen and influence on conduction mechanism through ta-C layer.

In order to find band gap values, both samples were characterized by means of STM (Figure 3). It was shown that ta-C layers from IMP-ta-C and REF-ta-C samples have the band gap values of 0.3 eV and 0.52 eV, which is extremely low value for ta-C layer. However, in the case of the sample with 30 nm thick ta-C layer deposited on top of sputtered Ti (under the same deposition conditions as used to fabricate the IMP-ta-C sample), the band gap value is 1.55 eV, which is in accordance with the results presented in [29,30]. Low values of band gaps for IMP-ta-C and REF-ta-C layers can be connected with high amount of $sp^2$ fraction in thin film samples as has been demonstrated in [31,32]. According to [32] there is a critical value for the ta-C layer thickness which must be reached for the stabilization of $sp^3$ matrix containing the distorted $sp^2$ bonds. This has been estimated to be in the range of 1-10 nm [32]. The thickness values of ta-C layer of IMP-ta-C and REF-ta-C are 7 and 15 nm, which means that the film properties are most likely quite far from those of bulk materials. In addition, we have recently shown by utilizing detailed density functional theory (DFT) calculations that the electronic properties of the DLC surface are considerable different from those of the “bulk” DLC [33]. In this case, as the film thickness is very small, the fraction of the surface out of the total DLC layer is significant and different electrical behavior in comparison to thicker DLC films can be expected.

It should be noted that, because compared samples have different thickness it is difficult to compare their properties only by the band gap values. Thus, XRR and Raman characterization were done. The results from XRR measurements showed that the ta-C density of of IMP-ta-C and REF-

ta-C samples were 3.2 and 3.05 g/cm$^3$, according to [34], such values of the ta-C layer density relates to high amount of sp$^3$ fraction (at the level of 85 and 60% for IMP-ta-C and REF-ta-C, respectively). However, it should be noted that in case of thin films (for example, as thin as 7 nm) XRR simulations can induce significant error for the density values, especially if the surfaces of the samples are rough, as is the case here. Thus, to further probe the similarities and differences between the two films, Raman measurements were carried out. Results of Raman spectroscopy are presented in Figure 4. The main feature of the spectrum is that the total intensity arising from the IMP-ta-C sample is higher than that from the REF-ta-C sample. As the thickness of the former is smaller, the difference in the signal intensity is probably connected at least to some degree with higher amount of sp$^2$ phase in IMP-ta-C. This is in contradiction with the XRR result, but as discussed above it is possible that the rough surface of the IMP-ta-C sample causes significant error to the XRR simulations. The ratio of intensities I(D)/I(G), which correlates with the band gap value and sp$^3$ fraction, are 0.84 and 0.37 for the IMP-ta-C and REF-ta-C samples, respectively. These values indicate that IMP-ta-C sample has narrower band gap and more sp$^2$ fraction in comparison to REF-ta-C consistent with data from STM measurements. It is, however, unlikely that the sp$^3$ content of IMP-ta-C would be as low as indicated by Raman results. This issue is addressed in more detail below.

To summarize the somewhat contradicting results shown above, it can be stated that 7 nm thick ta-C layer of IMP-ta-C sample is characterized by a very narrow band gap of 0.3 eV and higher amount of sp$^2$ fraction. Current conduction mechanism through such sample is caused by space-charge-limited current in the presence of monoenergetic traps with energy of 0.029 eV. On the other hand, 15 nm thick REF-ta-C sample is characterized by a wider band gap of 0.52 eV and smaller amount of sp$^2$ fraction. Current conduction mechanism through such sample is expected to be caused by space-charge-limited current in the presence of exponentially distributed traps with energies between 0.047-0.085 eV. Finally it should be noted that the variation of the oxygen content of the underlying Ti layers between the two types of films may also contribute to the observed differences in the electrical properties.

Based on what has been stated above, it can be stated that DC sputtering and cathodic arc deposition of Ti adhesion layer lead to (a) differences in the topography of the Ti and the topmost DLC layer and (b) orders of magnitude difference in local currents flowing through the electrode structure as measured by C-AFM. Related to the latter statement, it was observed that in the case of electrode structure consisting of 20 nm Ti layer deposited via pulsed cathodic arc deposition and 7 nm of improved DLC layer, the average current dropped dramatically to 20 pA (at 2 V of applied

voltage) in comparison to the same sample with DC magnetron sputtered Ti, which showed an average current of 18 nA with the same bias voltage. In order to investigate further the role of impurities (most importantly that of oxygen) and the effects of other film parameters on the observed phenomena several additional synthesis experiments were carried out and the obtained films analyzed by AFM/C-AFM. The outcome of these experiments can be summarized as follows: (i) as the *thickness* of the DLC layer (either IMP-ta-C or REF-ta-C) is *decreased* the *average current flowing through the electrode structure is increased*. The measured average current decreases exponentially from 14.9 nA to 83 pA as DLC thickness is changed from 4 to 30 nm (Figure 5). With this respect it should be remembered that the thickness of the ta-C films were 7 and 15 nm for the first (IMP-ta-C) and for the second (REF-ta-C) samples during the C-AFM measurements discussed above. (ii) *DC magnetron sputtered Ti* layer leads in general to *higher surface roughness* and *higher average currents* going through the sample structure, in comparison to cathodic arc deposited Ti layer. (iii) If the *Ti layer is allowed to excessively oxidize* before the deposition of DLC over layer, the *measurable average current* through the electrode structure *decreases* markedly, thus highlighting the role of excess impurities in the observed phenomena. It was observed that when using an *oxidized DC magnetron sputtered Ti*, the *average current* through the electrode structure *decreased* from 18 nA to 1.04 nA (at applied voltage of 2 V) in comparison to the non-oxidized layer. Further, it should be noted that such dependence was not observed for the samples with oxidized or non-oxidized Ti layers obtained by pulsed cathodic arc deposition. In the latter case the average current through the electrode structure was always at the level of 20-50 pA. This suggests that the cathodic arc deposited Ti layer may contain more impurities than the DC magnetron sputtered Ti after processing. In order to further clarify the structural and compositional differences between the two layers, detailed TEM analyses combined with EELS were carried out.

The STEM-HAADF image shown in Figure 6 (a) indicates that the Ti/Si interface is smooth whereas the Ti/DLC(IMP-ta-C) interface is relatively rough due to the surface morphology of the Ti layer. HRTEM image (Figure 6 b) shows that the Ti layer is polycrystalline with an average grain size of approximately 5 nm, whereas the DLC(IMP-ta-C) layer is completely amorphous. Thus, these observations further confirm the results from the above AFM studies (see Figure 1), which indicated that DC magnetron sputtered Ti layer has higher surface roughness than the corresponding layer deposited with cathodic arc. Further, STEM-HAADF image (Figure 6a) shows that the DLC (IMP-ta-C) surface is also rough but to a lesser degree than the Ti/DLC(IMP-ta-C) interface. Furthermore, HRTEM images also show that there is a 2 nm amorphous oxide layer between the Ti and the Si (Figure 6 b). EELS spectra taken at region 1 marked in the Figure 6 (a) at the

DLC(IMP-ta-C)/Ti interface as well as the EELS spectra taken at region 2 marked in the same figure (corresponding to the Ti/Si interface) both show a peak at the oxygen K-edge, confirming the presence of oxygen at both interfacial regions. Owing to the small thickness of the layers it was not possible to quantify the amount of oxygen. STEM-EELS was carried out on the IMP-ta-C to determine the proportion of $sp^2$-bonded carbon atoms present in the layer. A $C_{60}$ EELS spectra was taken as the reference [35] and the proportion of $sp^2$-bonded carbon atoms was calculated using the method reported by Cuomo *et al.* [36]. The atomic fraction of $sp^2$ bonded carbon ($x$) was calculated using the formula:

$$[I\pi/I\sigma]film/[I\pi/I\sigma]reference = 3x/(4-x) \quad (1)$$

where $I\pi$ and $I\sigma$ are the integrated intensities in the ranges 284 - 289 eV and 290 - 305 eV, respectively. Maximum of 30 ± 10 % carbon atoms present in the IMP-ta-C film were found to be $sp^2$-bonded, confirming that this is a high $sp^3$–content carbon film consistent with the XRR results. This also indicates that vis-Raman results obtained from thin film samples may significantly overestimate the $sp^2$ fraction of our films.

From Figures 6 (c) and (d) one can see that the DLC( REF-ta-C) film is also fully amorphous and its surface is very flat. The interfaces between layers are also relatively sharp and the underlaying Ti layer is uniform. It is also clear that an amorphous layer, which contains oxygen, has been formed at Si/Ti and Ti/DLC interfaces also in this case. Again the small layer thickness prevented any quantitative analysis of the oxygen content. The EELS spectra obtained at the carbon K-edge from the DLC(REF-ta-C) layer indicate that a high proportion of the carbon is present in the $sp^3$ bonding configuration also in this material, which is consistent with our previous results from the same material [4].

Conclusions based on the AFM, C-AFM and TEM/EELS results are the following: (i) both DLC layers are completely amorphous, (ii) they have high $sp^3$ contents, (iii) Ti layer deposited with DC magnetron sputtering is more rough (under IMP-ta-C) than Ti layer deposited with cathodic arc (under REF-ta-C). This is subsequently reflected in the higher surface roughness of the IMP-ta-C layer in comparison to that of REF-ta-C, (iv) during the C-AFM measurements the average current through the IMP-ta-C surface is much higher than that of REF-ta-C, (v) the presence of oxygen containing layers at the Si/Ti and Ti/DLC interfaces is evident in both electrode structures after processing, and (vi) the thickness of the IMP-ta-C layer used in the electrochemical measurements

is smaller (about 7 nm) than that of REF-ta-C (about 15 nm). This will have an effect of the electrical properties of the DLC layers as shown in Figure 5.

*3.2 Electrochemical properties*

As was discussed above, the use of thin DLC as the top electrode layer together with DC-sputtered Ti interlayer, can be expected to improve the electrochemical performance of the electrode structures. Therefore, two electrode structures, namely IMP (Si/DC-sputtered Ti-20 nm/ta-C-7nm) and the benchmark REF (Si/cathodic arc Ti-20 nm/ta-C-15 nm), were chosen for detailed electrochemical characterization. The cyclic voltammograms for the two types of electrode structures obtained in 0.15 M $H_2SO_4$ solution with cycling speed of 400 mV/s are shown in Figure 7 (a). As can be seen from the figure, both films are very stable and behave almost identically. The potential window for IMP is $\Delta E_{sweep}$ = 3.5 V and for REF, $\Delta E_{sweep}$ = 3.7 V. The current threshold level used for this was 200 µA. The capacitive background currents are also almost identical and reasonable small in both cases. Capacitance values were calculated at 0 V and with cycling speed of 50 mV/s and 400 mV/s. Geometric area of the electrode was used in the calculations and the difference between the anodic and cathodic current densities was used ($\Delta i = 2 \times C \times v$). The value obtained for the IMP is 44.8 ±13.4 µF/cm$^2$ and that for REF is 62.2±18.6 µF/cm$^2$. Lowest reported values for DLC are 3.45 µF/cm$^2$ for nitrogen doped DLC fabricated by sputtering and 1.02 µF/cm$^2$ for DLC fabricated by Filtered Cathod Vacuum Arc (FCVA) method [37,38]. Typical values reported for boron doped diamond (BDD) electrodes vary between 3.7 and 7.1 µF/cm$^2$ [39] and that for glassy carbon is generally about 30 µF/cm$^2$ [40]. In our case there is no really clear flat double layer region, as there is small but continuous increase in current as a function of potential throughout the "linear" region. This indicates that there are most likely oxygen containing groups present at the DLC surface which impose faradic currents on top of the actual charging current, thus explaining the higher than expected capacitance values and high error margins. The TEM analysis indicated that in both electrode structures oxygen is present inside the thin layers. In addition, X-ray photoelectron spectroscopy measurements (not shown here) showed that there is a relatively high amount of oxygen present at the surface of both IMP and REF after processing and in the latter (REF) the oxygen content was higher than that of IMP. Zeta potential measurements (results not shown here) gave pH 2.6 as the isoelectric point for the IMP-ta-C. These results together point out that there should be acidic functional groups on the surface of IMP-ta-C film, which most likely are carboxylic acid and hydroxyl groups. Finally there was hardly any change in the electrochemical

window as a function of number of cycles. Therefore, it can be stated that both types of amorphpous carbon films are inert and stable under the above tested conditions.

The electron transfer properties of the electrodes were subsequently probed by using the ferrocene redox couple. It is known to be a so called outer sphere redox couple [2] and its electron transfer rate should not therefore be influenced by the surface properties of the electrode. From Figure 7 (b) it can be seen that despite the almost identical potential windows and capacitive background currents, the two types of amorphous carbon films exhibit highly different behavior with respect to electron transfer. When the electron transfer is reversible the separation between the anodic and cathodic peaks will be 59 mV in this one electron transfer redox reaction. In addition, in the reversible case the peak separation does not change as a function of cycling speed. As can be seen from Figure 7 (b) and Table 1 the peak separation with 50 mV/s cycling speed is about 72 mV and with 400 mV/s cycling speed about 101 mV/s for the IMP-ta-C films. This behaviour can be qualified as quasi-reversible with a reasonable high electron transfer rate constant. On the other hand, the peak separations with the REF-ta-C film are about 220 mV and 352 mV with cycling speeds of 50 mV/s and 400 mV/s, respectively. In this case, the system can also be rated as quasi-reversible, but with a much lower electron transfer rate constant Thus, based on the above results there is a large difference in the electron transfer properties between the two films. This is also reflected in the fact that the peak separation changes more strongly as a function of cycling speed with the REF-ta-C electrode when compared to IMP-ta-C, further underlying the more irreversible nature of the REF-ta-C electrode.

### *3.3. Sensitivity of the two types of DLC electrodes towards dopamine (DA)*

To find out if the observed difference in the electron transfer rates would be seen also in the required sensor performance, the sensitivity of the two electrode structures (IMP and REF) towards dopamine was determined. Figures 8 - 10 and Table I show the results obtained from the measurements. As can be seen, when the concentration of dopamine is 1 mM the behavior of the two types of electrodes is quite similar (Fig. 8 (a)-(d)). During the first cycle starting to the anodic direction, there is a large oxidation peak and two reduction peaks that are clearly visible. During the second cycle also another oxidation peak appears around -0.1 V and 0.1 V in IMP-ta-C and REF-ta-C, respectively (Fig. 9 (a)-(d)). This is an oxidation peak related to the product formed in the oxidation process during the first cycle, which remained attached on the electrode surface. When cycling speed is changed from 50 mV/s to 400 mV/s there are clear changes both in the peak positions and $\Delta E_p$ for DA with the REF-ta-C electrode, whereas there is much smaller change in

the case of IMP-ta-C (Table I). Note here that the peak separation is calculated only for the DA oxidation peaks and the other reactions have not been considered (see discussion below). This clearly indicates that oxidation of DA on the surface of the ta-C electrode is more irreversible in comparison to that on top of IMP-ta-C. When cycling is continued with cycling speed of 50 mV/s it appears that both electrodes (IMP-ta-C and REF-ta-C) become completely passivated owing to some adsorbed species, but if the cycling speed is 400 mV/s this passivation does not occur (Figure 9 (a)-(d)), but intead a "steady state" behavior is achieved. Thus, behavior of dopamine on top of these amorphous carbon electrodes is seen to be quite complex. This issue will be addressed in more detail later on.

When the concentration of DA is decreased to 100 µM it is seen that the two oxidation waves can still be seen with both electrodes if the cycling speed of 400 mV/s is used starting from the second cycle (Figure 9 (a) and (b)). Nevertheless, as seen from the figures the first oxidation peak is not clear with either one of the electrodes. It is a bit easier to see the first peak with IMP-ta-C, but in the case of REF-ta-C it is really hard to be observed. It is nevertheless evident that both types of films can detect 100 µM of DA. The positions of the oxidation peaks are however different between the two electrodes. In the REF-ta-C case the most notable rise in current is around 350 mV (vs. Ag/AgCl) when cycling speed of 50 mV/s is used. On the other hand, with IMP-ta-C electrode the peak is situated at 190 mV (vs. Ag/AgCl), which is lower than that observed with Pt electrodes under the same conditions [4]. With cycling speed of 400 mV/s the peak positions are at 440 mV and at 220 mV, for REF-ta-C and IMP-ta-C respectively (Fig. 9). When the concentration is further decreased, REF-ta-C cannot detect DA anymore. However, IMP-ta-C can still detect DA when its concentration is as low as 1 µM (Fig. 10). With this concentration one can still see peaks for both oxidation and reduction in the corresponding voltammogram. It is also clear that there is only one oxidation peak visible for these low concentrations of the reactants present in the solution. Based on the above discussion, it can be concluded that there is at least two orders of magnitude difference in the sensitivity between these two structurally quite similar DLC thin film electrodes.

### *3.4. Reaction scheme for dopamine (DA) on top of the DLC electrodes*

Dopamine reaction has been suggested to be ECE, ECC or ECECEE [19,41-43] and fouling of Au electrodes, for example, has been observed to take place during electrochemical measurements. This type of behavior is also evident in this case (Figure 9 (a) –(d)). The following sequence is suggested to take place when electrodes (IMP-ta-C and REF-ta-C) are cycled in PBS solution containing 1 mM of DA with 50 mV/s. During the first cycle, DA is oxidized to dopaminequinone

(DAQ), which is then chemically reacted to leucodopaminechrome (LDAC). Owing to the high overpotential LDAC is oxidized immediately to dopaminechrome (DAC), as the anodic scan continues (the peak like feature around 1.2 V). During the reverse cycle we can see two reduction peaks out of which the first one is assigned to the reduction of DAQ to DA and the second one to the reduction of DAC to LDAC. When the second anodic cycle is started, we can see the appearance of another peak, which corresponds to the oxidation of LDAC to DAC. The main peak, which corresponds to the oxidation of DA is also clearly visible, but slightly reduced in size. Based on the cyclic voltammograms carried out with 50 mV/s, it appears that at least part of the DAC formed is adsorbed on the surface of the electrode and undergoes further chemical reaction, which leads to the formation of a passivating surface film. However, if the cycling speed is 400 mV/s polymerization does not have time to occur and reach a "steady state" where two oxidation and two reduction peaks remain visible in the voltammogram. The effect of cycling speed seen here is consistent with the finding of Li et al. [43] while working with Au electrodes. When concentration of DA is reduced to 100 µM it appears that the amount of DAQ that reacts chemically into LDAC is not high enough anymore to clearly observe the oxidation peak to appear this result being consistent with the results in [43] Thus, we see clearly only one oxidation and one reduction peak with both electrodes (Fig. 10). When concentration is further reduced down to 1 µM, it is clear that there is only one peak left, which is related to oxidation of DA. Thus, the observed passivation of the electrode surface may not be an issue, except in long term use, in the actual in vivo applications, where the concentrations of dopamine are below micromolar range.

## 4. Conclusions

We have shown above that by inducing topography on the DLC thin film surface and controlling the film thickness, it is possible to increase electron transfer properties and sensitivity towards dopamine while *at the same time* maintaining the wide water window and low capacitive background current characteristic of the high $sp^3$ containing and hydrogen free DLC electrodes. By using our previous DLC thin films as the benchmark, the following conclusions can be made based on the experimental results: (i) the new improved DLC film (IMP-ta-C) is a high $sp^3$ containing amorphous carbon film and thus similar in this respect to our previous REF-ta-C DLC-films, (ii) surface of the IMP-ta-C films is rougher in comparison to the REF-ta-C surface used here as the benchmark. These topographical differences between the two films are caused by the morphology of the two different types of Ti interlayers used between Si and DLC. (iii) The roughness difference is reflected in the local electrical properties of the IMP-ta-C and REF-ta-C surfaces, the former being orders of magnitude more conductive than the latter. It should be noted here, however, that

the smaller thickness of the IMP-ta-C layer in comparison to REF-ta-C layer will also contribute to the observed conductivity difference. (iv) Both DLC films (IMP-ta-C and REF-ta-C) exhibit a very wide and stable electrochemical windows as well as reasonably low capacitive background currents. (v) There is a very large difference in the electron transfer properties of the two electrodes and IMP-ta-C has much more facile electron transfer kinetics than REF-ta-C. (vi) The difference in the electron transfer kinetics is also reflected in the sensitivity towards dopamine. IMP-ta-C can detect two oreders of magnitude lower concentrations of dopamine than REF-ta-C. (vii) It is shown that the dopamine undergoes complex electrochemical and chemical processes on top of these amorphous carbon electrodes, which under some circumstances leads to a complete passivation of the electrode. It should however, be noted that this behavior requires substantially higher concentrations of dopamine than present in the actual in vivo measuring environment. Finally it can be concluded that the present approach provides a promising and simple tool to improve the electrochemical sensitivity of amorphous carbon thin films and with optimization of the deposition processes further improvements in the sensitivity towards dopamine can be expected.

**Acknowledgements:**

The authors T.L, V.P., S.S., T.P., and J.K., would like to acknowledge the National Agency for Technology and Innovation and Aalto University for financial support. The author V.P. acknowledges the provision of facilities and technical support by Aalto University at Micronova Nanofabrication Centre and S. Sintonen for XRR measurements.

References:


1. Stamenkovics, V., Mun B., Arenz M., and Mayrhofer K., Trends in electrocatalysis on extended and nanoscale Pt-bimetallic alloy surfaces. Nature Materials 2007; **6**: 241-247.
2. McCreery R. Advanced carbon electrode materials for molecular electrochemistry. Chem. Rev. 2008; **108***:* 2646-2687.
3. J. Robertson, Diamond-like amorphous carbon. Mater. Sci. Engineer., 2002; **37**(4-6): 129-281.
4. Laurila T., Rautiainen A., Sintonen S., Jiang H., Kaivosoja E., and Koskinen J., Diamond-like carbon (DLC) thin film bioelectrodes: Effect of thermal post treatments and the use of Ti adhesion layer. Mater. Sci. Engineer. C. 2014; **34:** 446-454.
5. Allen, M. Myer, B. & Rushto, N. In vitro and in vivo investigations into the biocompatibility of diamond- like carbon (DLC) coatings for orthopedic applications. J. Biomed. Mater. Res.2001; 58, 319-328.
6. Kaivosoja E, Myllymaa S, Takakubo Y, Korhonen H, Myllymaa K, Konttinen YT, Lappalainen R and Takag M. Osteogenesis of human mesenchymal stem cells on micro-patterned surfaces. J. biomater. Appl.,2011; **27:** 862-871.
7. Kaivosoja E, Suvanto P, Barreto G, Aura S, Soininen A, Franssila S and Konttinen YT. Cell adhesion and osteogenic differentiation on three dimensional pillar surfaces. J Biomed Mater Res Part A. 2012; 101: 842-852.
8. Myllymaa S., Kaivosoja E.,Myllymaa K.,Sillat T., Korhonen H.,Lappalainen R., and Konttinen, YT. Adhesion, spreading and osteogenic differentiation of mesenchymal stem cells cultured on micropatterned amorphous diamond, titanium, tantalum and chromium coatings on silicon. J Mater Sci: Mater Med. 2012: **21:** 329-341.
9. Myllymaa K., Levonc J.,Tiainen V-M., Myllymaa S., Soininen A., Korhonen H., Kaivosoja, Lappalainen R., and Konttinen YT. Formation and retention of staphylococcal biofilms on DLC and its hybrids compared to metals used as biomaterials. ,Colloids and Surfaces B: Biointerfaces. 2013; **101:** 290-297.
10. Soininen, A. Tiainen V-M., Konttinen Y., van der Mei H., Busscher H., and Sharma P., J. Biomed. Mater. Res. Part B: Appl. Biomater. Bacterial Adhesion to Diamond-like Carbon as Compared to Stainless Steel. 2009; **90:** 882–885.
11. Grill A. Diamond-like carbon coatings as biocompatible materials—an overview. Diamon. Relat. Mater. 2003; **12**(2):166-170.

12. Schnupp R., Kuhnhold R., Temmel G., Burte E., and Ryssel H.. Thin carbon films as electrodes for bioelectronic applications. Biosensors Bioelectr., 1998; **13**(7-8):889-894.
13. Yoo K., Miller B., Kalish, R., and Shi X. Electrodes of Nitrogen-Incorporated Tetrahedral Amorphous Carbon: A Novel Thin-Film Electrocatalytic Material with Diamond-like Stability, Electrochem. Solid-State Lett., 1999; **2**: 233-235.
14. Yoo K., Miller B., Kalish, R., and Shi X. Copper Electrodeposition and Dissolution on Tetrahedral Amorphous Carbon Incorporating Nitrogen, J. Electrochem. Soc., 2001; **148**: C95-C101.
15. Sopchak, D., Miller, B., Kalish,R., Avyigal, Y., and Shi X., Dopamine and Ascorbate Analysis at Hydrodynamic Electrodes of Boron Doped Diamond and Nitrogen Incorporated TetrahedralAmorphous Carbon, Electroanalysis, 2001; **14**: 473-478.
16. Tanaka Y., Furuta, M., Kuriyama, K., Kuwabara R., Katsuki Y., Kondo, T., Fujishima, A., and Honda K., Electrochemical properties of N-doped hydrogenated amorphous carbon films fabricated by plasma-enhanced chemical vapor deposition methods, Electrochemica Acta, 2011; **56**: 1172–1181.
17. Patel,A., McKelvey, K., and Unwin P., Nanoscale Electrochemical Patterning Reveals the Active Sites for Catechol Oxidation at Graphite Surfaces., J. Am. Chem. Soc., 2012; **134**: 20246−20249.
18. Beaulieu J. M., and Gainetdinov R. R.The Physiology, Signaling, and Pharmacology of Dopamine Receptors, Pharmacol. Rev. 2011; **63**: 182-217.
19. Chumillas S, Figueireido M., Climent V., and Feliu J. Study of dopamine reactivity on platinum single crystal electrode surfaces, Electrochemica Acta 2013; **109**: 577-586.
20. Venton, J. B. & Wightman, M. R. Psychoanalytical Electrochemistry: Dopamine and Behaviour. Analytical Chemistry. 2013; **75:** 414-421.
21. Guo D.-Z., Hou S.-M., Zhang G.-M., and Xue Z.-Q., Conductance fluctuation and degeneracy in nanocontact between a conductive AFM tip and a granular surface under small-load conditions, Appl. Surf. Sci., 2006; **252**: 5149–5157.
22. Butt, H.-J. Cappella Br., Kappl M., Force measurements with the atomic force microscope: Technique, interpretation and applications, Surface Science Reports, 2005; **59**: 1–152.
23. Frammelsberger W., Benstetter G., Kiely J., Stamp R., C-AFM-based thickness determination of thin and ultra-thin $SiO_2$ films by use of different conductive-coated probe tips, Appl. Surf. Sci., 2007; **253**: 3615–3626.
24. Protopopova V., Laurila T., Palomäki T., and Koskinen J., Electronic properties and conduction mechanism through Ti / ta-C bilayer structures (submitted)

25. May P.W., Kuo M.-T., Ashfold M.N.R., Field emission conduction mechanisms in chemical-vapour-deposited diamond and diamond-like carbon films, Diamond Rel. Mater., 1999; **8:** 1490–1495.
26. Martinez-Vega J. (Ed.) Dielectric Materials for Electrical Engineering, John Wiley & Sons, Inc., Hoboken, NJ USA, 2013.
27. Harada, T. Ohkubo I., Tsubouchi K., Kumigashira H., Ohnishi T., Lippmaa M., et al., Trap-controlled space-charge-limited current mechanism in resistance switching at $AlPr_{0.7}Ca_{0.3}MnO_3$ interface, Appl. Phys. Lett. 2008; **92**: 222113–1–3.
28. Cheong K.Y., Moon J. H., Kim H. J., Bahng W., and Kim N.-K., Current conduction mechanisms in atomic-layer-deposited $HfO_2$/nitrided $SiO_2$ stacked gate on 4H silicon carbide, J. Appl. Phys. 2008; **103**: 084113–1–8.
29. Rusman I., Klibanov L., Burstein L., Rosenberg Yu., Weinstein VBen-Jacob, E., et al., Microstructure and phase characterization of diamond-like amorphous hydrogenated carbon films using STM/STS, Thin Solid Films 1996; **287**: 36–44.
30. Arena C., Kleinsorge B., Robertson J., Milne W.I., and Welland M.E., Electronic and topographic structure of ta-C, ta-C:N and ta-C:B investigated by scanning tunnelling microscopy, Diamond Rel. Mater. 1999; **8**: 435–439.
31. Ivanov-Omskii V.I., Tolmatchev A.V., and Yastrebov S.G., Optical study of amorphous carbon films deposited by magnetron sputtering of graphite, Semiconductors, 2001; **35**: 220–225.
32. Soin N., Roy, S.S., Ray S.C., Lemoine P.,. Rahman Md.A, Maguire P.D., et al., Thickness dependent electronic structure of ultra-thin tetrahedral amorphous carbon (ta-C) films, Thin Solid Films, 2012; **520**: 2909–2915.
33. Caro M., Zoubkoff R, Lopez-Acevedo O., and Laurila T, "Atomic and electronic structure of tetrahedral amorphous carbon surfaces from density functional theory: properties and simulation strategies", Carbon, (in print)
34. Ferrari A.C., Libassi A., Tanner B.K., Stolojan V., Yuan J., Brown L. M., et al., Density, $sp^3$ fraction, and cross-sectional structure of amorphous carbon films determined by x-ray reflectivity and electron energy-loss spectroscopy, Phys. Rev. B : 2000; **62**: 089–11 103.
35. Alexandrou I., Scheibe H.-J., Kiely C. J., Papworth A. J., Amaratunga G. A. J., and Schultrich B. Carbon films with an sp2 network structure. Phys. Rev. B 1999; 60: 10903-10907.
36. Cuomo J. J., Doyle J. P., Bruley J., and Liu J. C. Sputter deposition of dense diamond- like carbon films at low temperature. Appl. Phys. Lett. 1991; **58**: 466-468.

37. Zeng, A., Liu E., Tan S. N., Zhang S., and Gaoa J. Cyclic Voltammetry Studies of Sputtered Nitrogen Doped Diamond-Like Carbon Film Electrodes. Electroanalysis. 2002; **14**: 1110-1115.
38. Liu E. and Kwek H.W. Electrochemical performance of diamond-like carbon thin films. Thin Solid Films. 2008; **516**: 5201-5206.
39. Swain G. M. and Ramesham A. The electrochemical activity of boron-doped polycrystalline diamond thin film electrodes. Anal. Chem. 1993; **65**: 345-351.
40. McDermott M. T., McDermott C. A., and McCreery R. L. Scanning tunneling microscopy of carbon surfaces: relationships between electrode kinetics, capacitance, and morphology for glassy carbon electrodes. Anal. Chem. 1993; **65**:937-944
41. Zen J., and Chen P., A selective voltammetric method for uric acid and dopamine detection using clay-modified electrodes. Anal. Chem. 1997; **69**: 5087-5093.
42. Wen X-L., Jia Y-H. and Liu Z-L. Micellar effects on the electrochemistry of dopamine and its selective detection in the presence of ascorbic acid. Talanta. 1999; **50**:1027-1033.
43. Li Y., Liu M., Xiang C., Xie Q., and Yao S.. Electrochemical quartz crystal microbalance study on growth and property of the polymer deposit at gold electrodes during oxidation of dopamine in aqueous solutions. Thin Solid Films. 2006; **497**:270-278

Figure and table captions:

Table 1 Summary of the electrochemical properties of the two types of DLC films.

Figure 1. Topography maps (a,d), current maps (b,e) and topography and current profiles (c,f) of the IMP (a,b) and REF (c,d) samples surface. Current maps were obtained under values of voltage applied to the probe equaled to 0.7 and 4.5 V for IMP and REF sampes.

Figure 2. Current-voltage curves obtained from conductive AFM of IMP and REF samples plotted in linear (a) and logarithmic coordinates (b).

Figure 3. Dependences of (a) the tunneling current and (b) the differential conductivity on the sample voltage for IMP, REF and sample with 30 nm thick top ta-C layer on sputtered Ti.

Figure 4. Raman spectra from IMP and REF samples.

Figure 5. Figure showing the change of average current as a function of the DLC thickness.

Figure 6. (a) Cross-sectional STEM-HAADF image showing a 7 nm DLC(IMP) layer on a Ti interlayer deposited on (100) silicon, (b) HRTEM image showing the amorphous DLC (IMP) layer on a rough polycrystalline Ti layer, (c) cross-sectional TEM image showing a 30 nm DLC (REF) on a Ti interlayer, and (d) HRTEM image showing the amorphous DLC (REF) on top of smooth polycrystalline Ti. (note: ta-C layer used in all other analyses than cross-sectional TEM was 15 nm thick).

Figure 7. Results from the cyclic voltammetry measurements showing (a) the water window in mild $H_2SO_4$ for the two types (IMP and REF) of DLC thin films and (b) the corresponding FcMeOH measurements.

Figure 8. Results from the cyclic voltammetry measurements showing the behaviour of the electrodes in 1 mM dopamine (DA) solution (a) REF first cycle, (b) IMP first cycle, (c) REF second cycle and (d) IMP second cycle.

Figure 9. Results from the cyclic voltammetry measurements showing the behaviour of the electrodes in 1 mM dopamine (DA) solution as cycling continues (a) REF 50 mV/s cycling speed, (b) REF 400 mV/s cycling speed, (c) IMP 50 mV/s cycling speed, and (d) IMP 400 mV/s cycling speed.

Figure 10. Results from the cyclic voltammetry measurements showing the sensitivity towards dopamine for (a) REF and (b) IMP thin film electrodes.

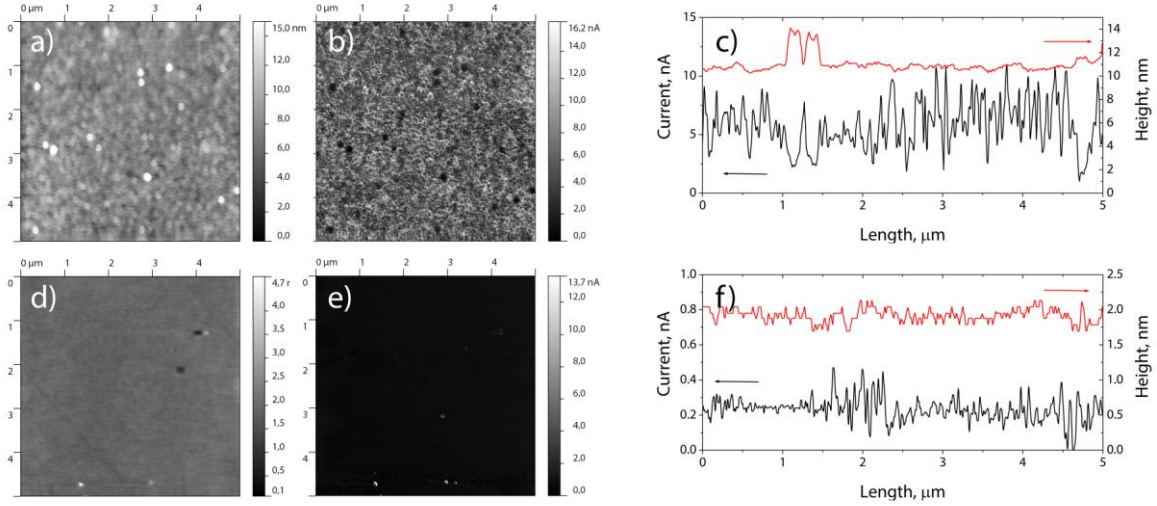


**Figure 1**

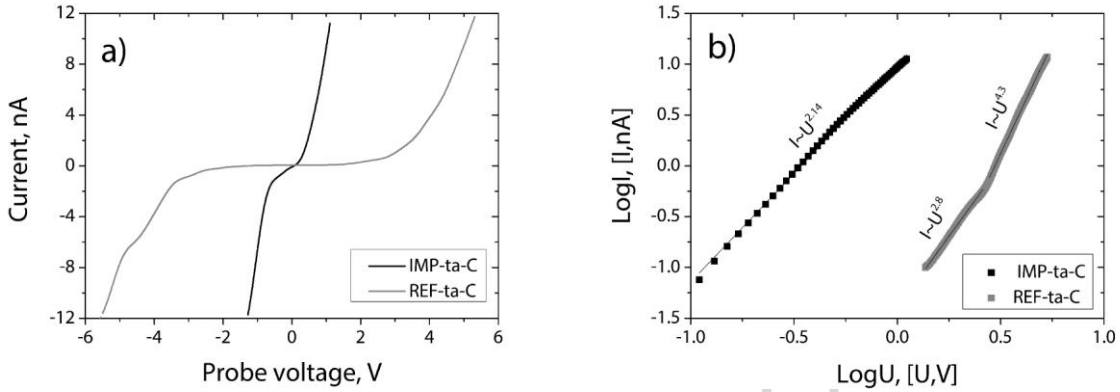


**Figure 2**

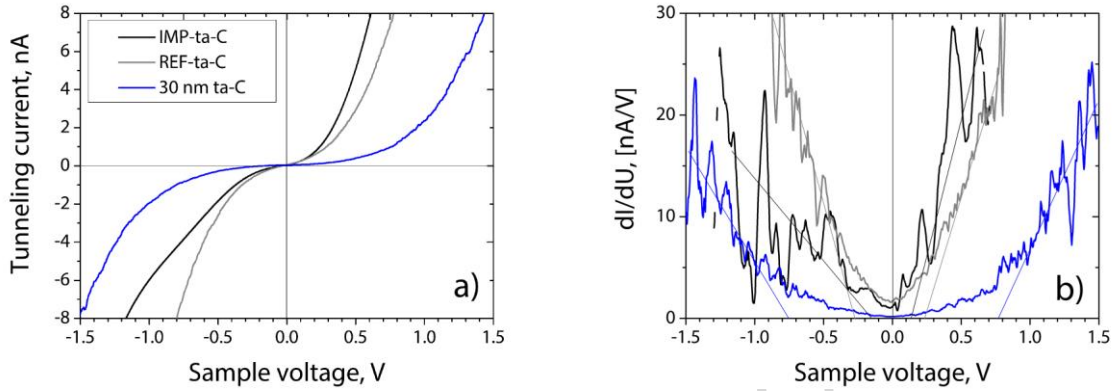


**Figure 3**

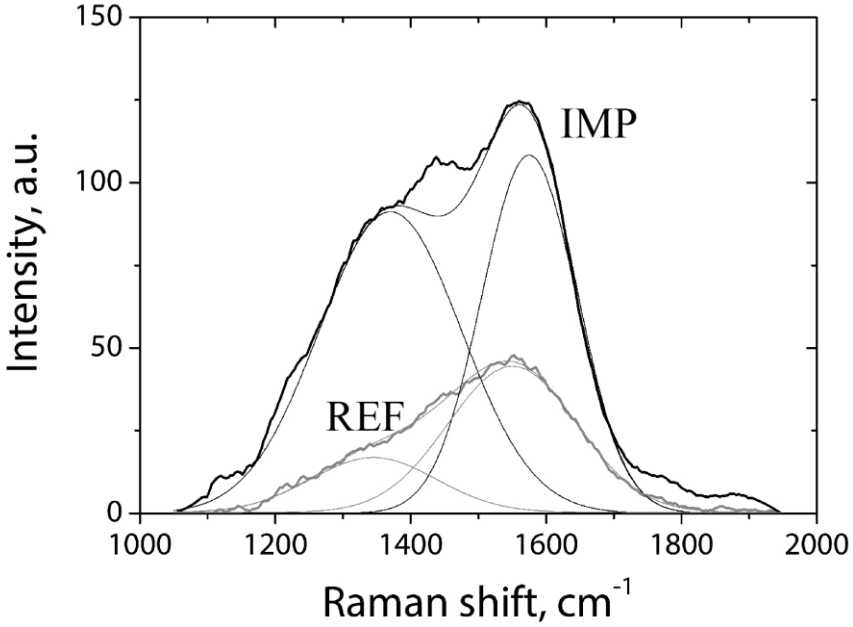


**Figure 4**

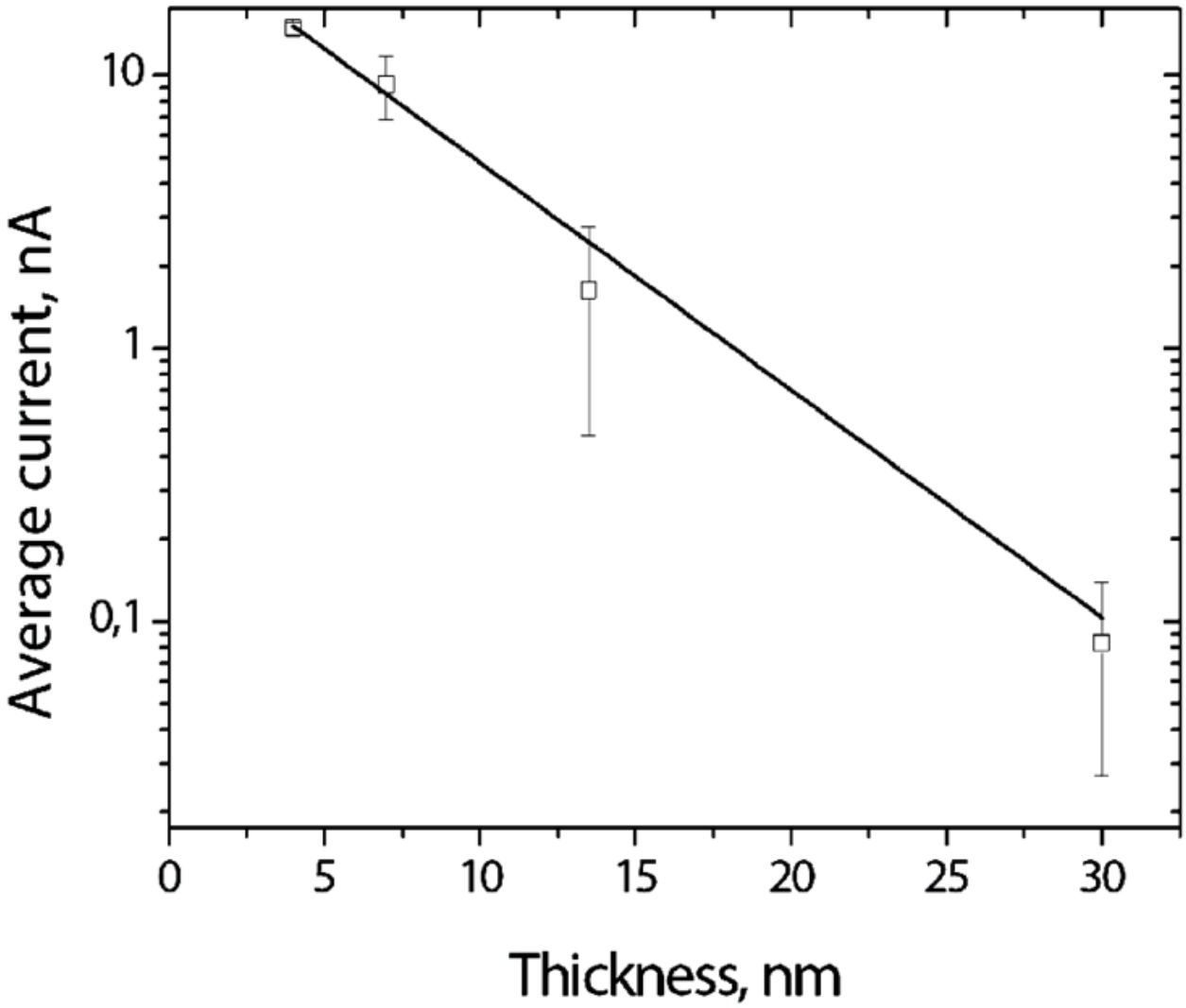


**Figure 5**

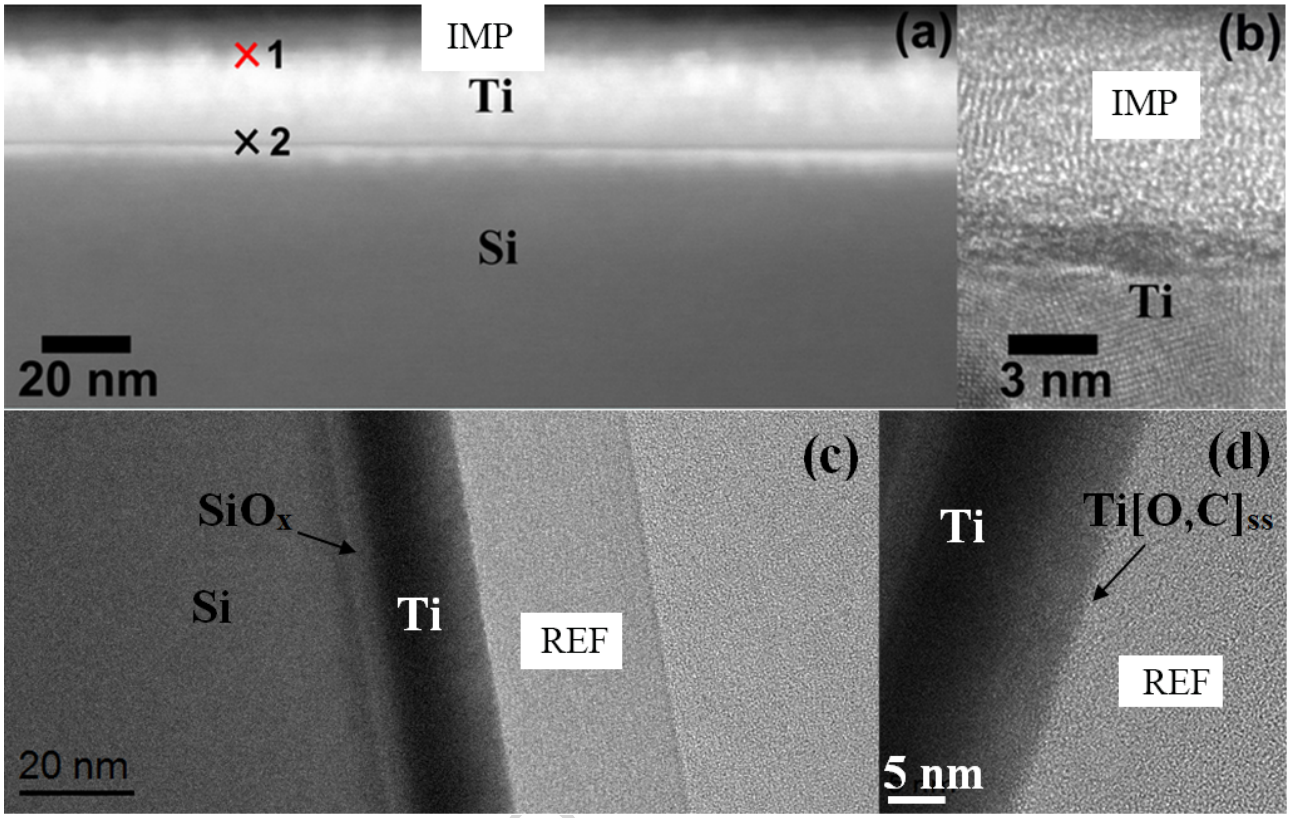


**Figure 6**

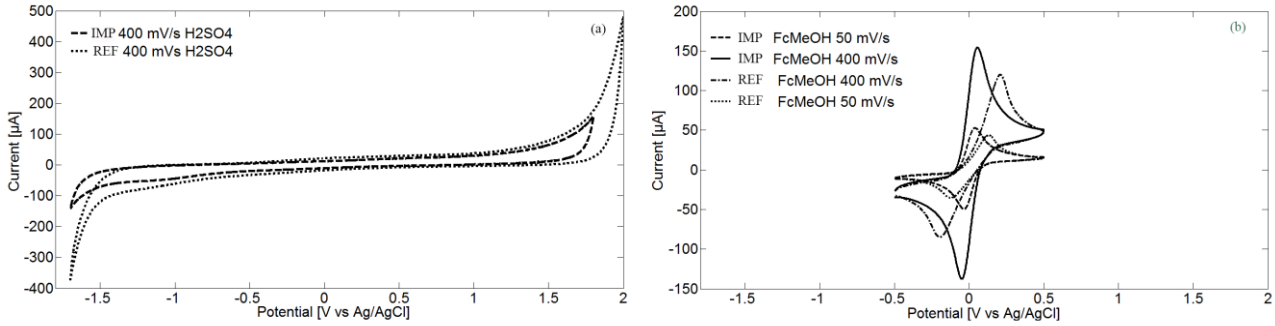


**Figure 7**

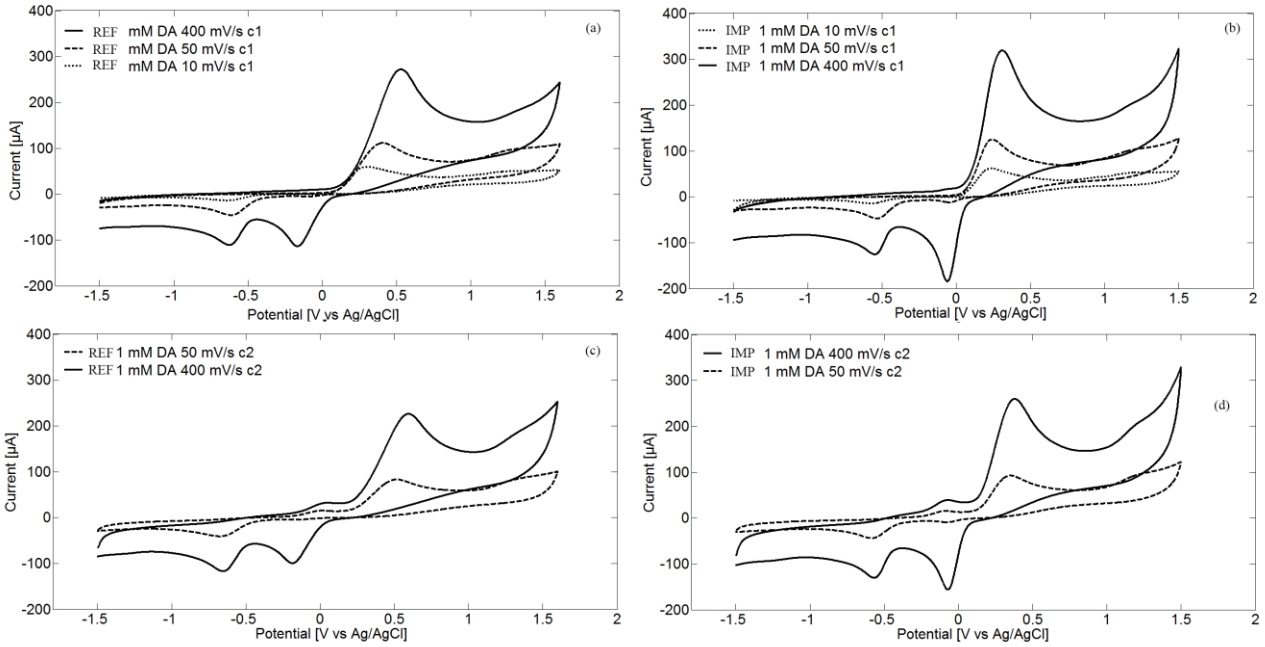


**Figure 8**

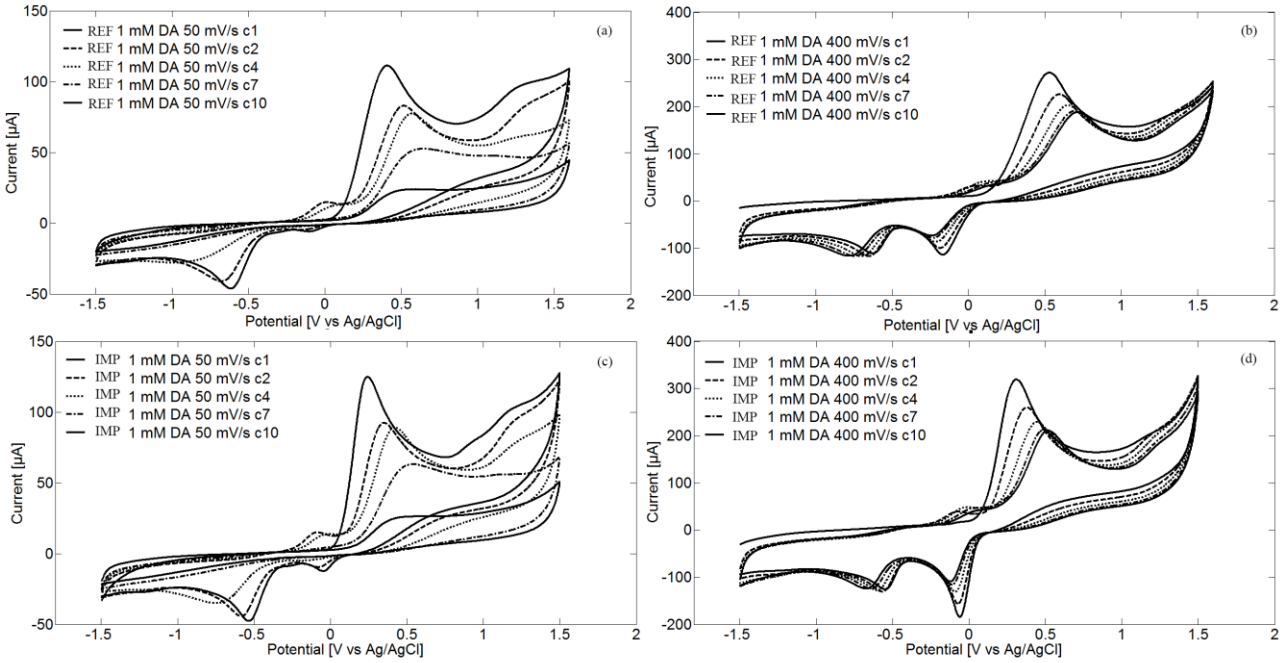


**Figure 9**

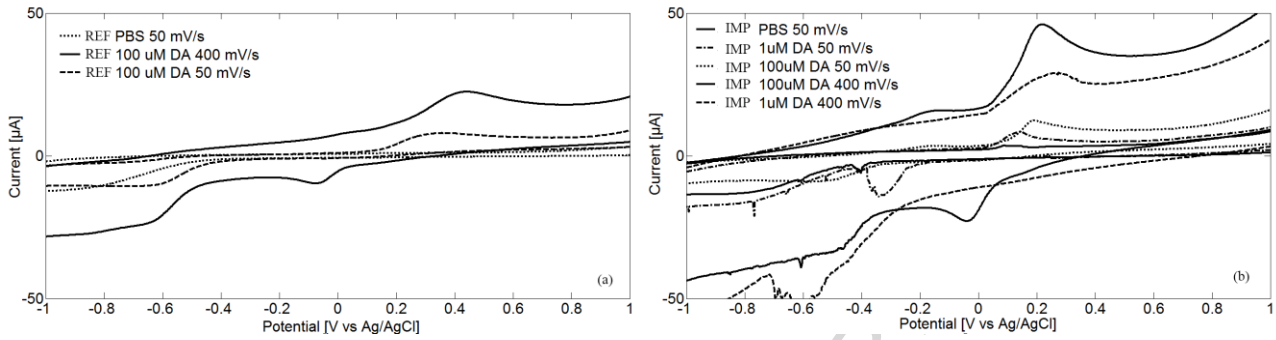


**Figure 10**

**Table 1**

| Electrode | Water Window ($H_2SO_4$) | Water Window (PBS) | Apparent double layer capacitance ($\mu F/cm^2$) | $\Delta E_p$ FcMeOH (50 mV/s) | $\Delta E_p$ FcMeOH (400 mV/s) | Detection limit (DA) | $\Delta E_p$ DA (50mV/s) | $\Delta E_p$ DA (400 mV/s) |
|---|---|---|---|---|---|---|---|---|
| **REF** | 3.7 V | 3.6 V | 62.2±18.6 | 262 mV | 402 mV | 100 µM | 500 mV | 696 mV |
| **IMP** | 3.5 V | 3 V | 44.8 ±13.4 | 72 mV | 101 mV | 1 µM | 286 mV | 370 mV |

**Primary novelty statement**

- The manuscript describes the synthesis and detailed structural and electrochemical characterization of a new high $sp^3$ containing, hydrogen free diamond-like carbon (DLC) material with a very wide and stable water window, reasonable low capacitive background current but, *at the same time,* very facile electron transfer kinetics and high sensitivity towards dopamine.
- By utilizing TEM, SEM, AFM, C-AFM and extensive cyclic voltammetry (CV) measurements, we have been able to demonstrate that the increase in the sensitivity towards dopamine and generally improved electrochemical properties of the material, can be mainly explained based on the surface topography and local electrical properties of the electrode structures.
- We also present for the first time (to our knowledge) quantitative data about the relation between the thickness of the nanometer scale DLC thin films and the measured average current flowing through the electrode structure.

Highlights

- Data about the influence of topography on the electrical properties of thin DLC films is provided
- In-depth discussion to explain the above dependency is included
- Electrochemical properties of the new DLC thin film electrodes are provided
- New DLC electrodes show two orders of magnitude increase in their sensitivity towards DA
- Dopamine is shown to exhibit complex reactions on top of these new DLC electrodes